

Resonances of the Frobenius-Perron Operator for a Hamiltonian Map with a Mixed Phase Space

Joachim Weber^{1,2}, Fritz Haake¹, Petr A. Braun^{1,3}, Christopher Manderfeld¹, and Petr Šeba⁴

¹ *Fachbereich Physik, Universität-GH Essen, 45117 Essen, Germany*

² *Department of Physics of Complex Systems, Weizmann Institute of Science, Rehovot 76100, Israel*

³ *Institute of Physics, Saint-Petersburg University, Saint-Petersburg 198504, Russia*

⁴ *Institute of Physics, Czech Academy of Sciences, Prague, Czech Republic*

(Date: October 28, 2018)

Resonances of the (Frobenius-Perron) evolution operator \mathcal{P} for phase-space densities have recently attracted considerable attention, in the context of interrelations between classical and quantum dynamics. We determine these resonances as well as eigenvalues of \mathcal{P} for Hamiltonian systems with a mixed phase space, by truncating \mathcal{P} to finite size in a Hilbert space of phase-space functions and then diagonalizing. The corresponding eigenfunctions are localized on unstable manifolds of hyperbolic periodic orbits for resonances and on islands of regular motion for eigenvalues. Using information drawn from the eigenfunctions we reproduce the resonances found by diagonalization through a variant of the cycle expansion of periodic-orbit theory and as rates of correlation decay.

I. INTRODUCTION

Chaotic behavior in classical Hamiltonian systems manifests itself in an infinite hierarchy of phase-space structures and instability of trajectories with respect to small changes in their initial condition. If resolution in phase space is restricted, e.g. due to finite precision of measurements, phase-space trajectories can be followed only approximately. Every finite-resolution initial condition actually stands for an entire ensemble of trajectories with possibly very different long-time behaviors. That fact suggests a probabilistic approach to the dynamics, in which a phase-space density and its propagator \mathcal{P} , the so called Frobenius-Perron operator, are studied.

Because of Liouville's theorem \mathcal{P} can be represented by an infinite unitary matrix in a Hilbert space of phase-space functions. The spectrum of \mathcal{P} thus lies on the unit circle in the complex plane. Discrete eigenvalues represent regular dynamics, while chaos entails a continuous spectrum, and along with the latter resonances of \mathcal{P} may occur that characterize effectively irreversible behavior [1,2]. Apart from their role as decay rates, Frobenius-Perron resonances have been found to link classical with quantum dynamics because they could as well be identified from quantum systems [3,4]. Furthermore, they have been predicted to carry information on the system-specific corrections to universality of quantum fluctuations [5,6].

To identify resonances, mathematically defined as singularities of the resolvent of \mathcal{P} in some higher Riemannian sheet, it is necessary to analytically continue the resolvent across the continuous spectrum of \mathcal{P} from the outside to the inside of the unit circle [7–9]. This becomes increasingly difficult as the dynamics gains complexity. Especially for the large class of systems with a mixed phase space an effective approximation scheme is needed that is free of restrictions of previous investigations [10,11], such as hyperbolicity, one-dimensional (quasi-) phase space, or isolation of the phase-space regions causing intermittency.

In the following we present such a scheme and illustrate it for a prototypical dynamical system with a mixed phase space, a periodically kicked top. We represent \mathcal{P} in a Hilbert space of phase-space functions as an infinite unitary matrix and subsequently truncate it to a finite N -dimensional matrix $\mathcal{P}^{(N)}$, with resolution in phase space as the truncation criterion. We thus generate a nonunitary approximation to the unitary \mathcal{P} that becomes exact as $N \rightarrow \infty$. Looking at the spectra of $\mathcal{P}^{(N)}$ with increasing N , we find some eigenvalues persisting in their positions, either almost on the unit circle or well inside, and we focus on these “frozen” eigenvalues. While frozen (near)unimodular eigenvalues of $\mathcal{P}^{(N)}$ turn into unimodular eigenvalues of \mathcal{P} as $N \rightarrow \infty$, the nonunimodular frozen eigenvalues are not part of the spectrum of \mathcal{P} in that limit. We will argue that at finite but large N they rather indicate the positions of resonances of \mathcal{P} . Accordingly, the eigenfunctions of $\mathcal{P}^{(N)}$ are of very different nature for these two cases. We find eigenfunctions to unimodular eigenvalues localized and approximately constant on islands of regular motion in phase space that are bounded by invariant tori. In contrast, eigenfunctions to nonunimodular eigenvalues of $\mathcal{P}^{(N)}$ are localized near unstable manifolds of hyperbolic periodic orbits. Just as nonunimodular eigenvalues are not in the spectrum of the Hilbert-space operator \mathcal{P} , the eigenfunctions are no Hilbert-space functions in the limit of infinite resolution. A comparison of the eigenfunctions of $\mathcal{P}^{(N)}$ for different values of N and furthermore with the eigenfunctions of the truncated inverse operator $\mathcal{P}^{-1(N)}$ illustrates why they lie outside the Hilbert space. The strong localization of these (resonance-)eigenfunctions at finite N allows us to identify the relatively few groups of periodic

orbits associated with a particular resonance up to a certain length. From only these orbits we recover resonances via a variant of the so-called cycle expansion of periodic-orbit theory that works even in the case of a mixed phase space. To verify that frozen eigenvalues have indeed the physical interpretation of resonances, we conclude with a numerical experiment in which the decay of a two-point correlation function is observed. In order to find a certain resonance responsible for correlation decay, the initial phase-space density is chosen localized in the phase-space region where the resonance-eigenfunction has large amplitudes.

A short account of the results to be discussed here has been published recently [12].

II. LIOUVILLE DYNAMICS ON THE SPHERE

As a prototypical Hamiltonian system with a phase space displaying a mix of chaotic and regular behavior we consider a periodically kicked angular momentum vector

$$(J_x, J_y, J_z) = (j \sin \theta \cos \varphi, j \sin \theta \sin \varphi, j \cos \theta) \quad (1)$$

of conserved length j , also known as the kicked top [13]. Such a system has one degree of freedom, and its phase space is a sphere. A phase-space point $X \equiv (p, q)$ may be characterized by an “azimuthal” angle φ as the coordinate q and the cosine of a “polar” angle θ as the conjugate momentum p . The dynamics is specified as a stroboscopic area preserving map, $X' = M(X)$. We chose M to consist of rotations $R_z(\beta_z), R_y(\beta_y)$ about the y - and z -axes and a “torsion”, i.e. a nonlinear rotation $T_z(\tau) = R_z(\tau \cos \theta)$ about the z -axis which changes φ by $\tau \cos \theta$,

$$M = T_z(\tau)R_z(\beta_z)R_y(\beta_y). \quad (2)$$

In the sequel we keep $\beta_z = \beta_y = 1$ fixed and vary the torsion constant τ to generate a phase space which is integrable for $\tau = 0$ and increasingly dominated by chaos as τ grows. We focus on $\tau = 2.1$ as a moderately chaotic case and $\tau = 10.2$ as strongly chaotic (see figures 1a,b), where elliptic islands have become so small that they are difficult to detect.

In the Liouville picture the time evolution of a phase-space density ρ is governed by Liouville’s equation,

$$\partial_t \rho = \mathcal{L} \rho = \{H, \rho\}, \quad (3)$$

where the Liouville operator \mathcal{L} , the Poisson bracket with the Hamiltonian H , appears as generator. For our rotations and torsion we separately take $H = \beta_y J_y, H = \beta_z J_z$, and $H = (\tau/2)J_z^2$. Denoting the respective Liouvillians by $\mathcal{L}_{R_y}, \mathcal{L}_{R_z}$, and \mathcal{L}_{T_z} we imagine Liouville’s equation for each of them integrated over a unit time span. The product of the resulting three propagators yields our Frobenius-Perron operator $\mathcal{P} = \exp(\mathcal{L}_{T_z}) \exp(\mathcal{L}_{R_z}) \exp(\mathcal{L}_{R_y})$. The action of \mathcal{P} on the phase-space density $\rho(q, p)$ can be represented in terms of the “Hamilton-picture” map M as

$$\begin{aligned} \rho_{n+1}(X) &= \mathcal{P} \rho_n(X) = e^{\mathcal{L}_{T_z}} e^{\mathcal{L}_{R_z}} e^{\mathcal{L}_{R_y}} \rho_n(X) \\ &= \int dX' \delta(X - M(X')) \rho_n(X'). \end{aligned} \quad (4)$$

Since the map M is invertible and area preserving, $\det \partial M(X)/\partial X = 1$, the integral simplifies to

$$\mathcal{P} \rho(X) = \rho [M^{-1}(X)]. \quad (5)$$

While a phase-space density is usually considered as L^1 -integrable it can be assumed to belong to a Hilbert space of L^2 -functions as well. The additional structure of the Hilbert space can be exploited to represent \mathcal{P} by an infinite unitary matrix, the unitarity $(\mathcal{P} \rho_1, \mathcal{P} \rho_2) = (\rho_1, \rho_2)$ following from (5) and area preservation in the map M . The basis functions may be chosen as ordered with respect to phase-space resolution. This allows us to eventually truncate \mathcal{P} to finite size and still retain the propagator intact for functions on large phase-space scales.

On the unit sphere the spherical harmonics $Y_{lm}(\varphi, \cos \theta)$ with $l = 0, 1, 2, \dots$ and integer $|m| \leq l$ form a suitable basis. Phase-space resolution is characterized by the index l : using all Y_{lm} with $0 \leq l \leq l_{\max}$ phase-space structures of area $\propto 1/l_{\max}^2$ can be resolved, and the number of these basis functions is $N = (l_{\max} + 1)^2$.

To check on the resolution achievable by spherical harmonics consider a Gaussian $G(\varphi, \theta) = \exp(-i(\varphi - \varphi_0)^2/\Delta\varphi^2 - i(\theta - \theta_0)^2/\Delta\theta^2)$ with the angular widths $\Delta\varphi, \Delta\theta$ and the effective area $\sim \Delta\varphi\Delta\theta$. To represent it by a linear combination of spherical harmonics we need only the Y_{lm} with $|m| \leq m_0 \sim 2\pi/\Delta\varphi$ and $l \leq 2\pi/\Delta\varphi + \pi/\Delta\theta$; all other spherical harmonics have negligible scalar product with $G(\varphi, \theta)$. Indeed, the effective

“wavelengths” of Y_{lm} in φ and θ are, respectively, $2\pi/|m|$ and $\pi/(l - |m|)$, the latter given by the number $(l - |m|)$ of zeros of the Legendre function P_{lm} in the interval $0 < \theta < \pi$; once these wavelengths become smaller than the respective widths $\Delta\varphi, \Delta\theta$ of the Gaussian the overlap of G and Y_{lm} is negligible. Inverting that statement we may say that a basis set of spherical harmonics cut off at a certain l_{\max} is suitable for representing objects on the unit sphere with the angular sizes $\sim l_{\max}$ and area $\sim l_{\max}^2$.

To obtain the matrix elements

$$\mathcal{P}_{lm, l'm'} = \int_{-1}^1 d\cos\theta \int_0^{2\pi} d\varphi Y_{lm}^*(\varphi, \cos\theta) Y_{l'm'} [M^{-1}(\varphi, \cos\theta)] \quad (6)$$

for the mixed dynamics it is convenient to first determine the Frobenius-Perron matrices for the two rotations $\exp(\mathcal{L}_{R_z}), \exp(\mathcal{L}_{R_y})$ and the torsion $\exp(\mathcal{L}_{T_z})$, all of which are by themselves integrable and free of chaos. Deferring the derivation to Appendix A we here just note the three matrices. The Frobenius-Perron matrix of the z -rotation is diagonal,

$$\left(\exp(\mathcal{L}_{R_z}) \right)_{lm, l'm'} = \delta_{ll'} \delta_{mm'} \exp(-im\beta_z). \quad (7)$$

For the y -rotation, $(\exp(\mathcal{L}_{R_y}))_{lm, l'm'}$ is blockdiagonal in l with the blocks well known from quantum mechanics as Wigner’s d-matrices,

$$\left(\exp(\mathcal{L}_{R_y}) \right)_{lm, l'm'} = \delta_{ll'} d_{mm'}^l(\beta_y). \quad (8)$$

For the z -torsion the Frobenius-Perron matrix elements are given by finite sums over products of spherical Bessel functions $j_l(x)$ and Clebsch-Gordan coefficients,

$$\begin{aligned} \left(\exp(\mathcal{L}_{T_z}) \right)_{lm, l'm'} &= \delta_{m, m'} (-1)^m \sqrt{(2l+1)(2l'+1)} \\ &\times \sum_{l''=|l-l'|}^{l+l'} (-i)^{l''} j_{l''}(m\tau) C_{0\ 0\ 0}^{l\ l'\ l''} C_{-m\ m\ 0}^{l\ l'\ l''}. \end{aligned} \quad (9)$$

Finally, for the mixed dynamics \mathcal{P} is the product of the three above matrices. Due to the Kronecker deltas involved, each element of \mathcal{P} is just the product of three matrix elements, one each for the rotations and the torsion. Obviously, \mathcal{P} is a full matrix coupling all phase-space scales, as it is to be expected for chaotic dynamics. We furthermore remark that with respect to the real basis

$$\begin{aligned} y_{l0} &= Y_{l0} \\ y_{lm}^+ &= \frac{1}{\sqrt{2}} (Y_{lm} + Y_{lm}^*), \\ y_{lm}^- &= \frac{1}{\sqrt{2i}} (Y_{lm} - Y_{lm}^*) \end{aligned} \quad (10)$$

the matrix \mathcal{P} is also real, since real phase-space densities cannot become complex under time evolution. As a consequence, all eigenvalues of $\mathcal{P}^{(N)}$ are either real or come in complex conjugate pairs.

III. RESONANCES AND EIGENVALUES AT FINITE PHASE-SPACE RESOLUTION

To study resonances and (discrete) eigenvalues of \mathcal{P} we investigate the finite-size approximants $\mathcal{P}^{(N)}$ for different values of N , i.e. different resolutions in phase space. In the low-resolution subspace spanned by the first N basis functions $\mathcal{P}^{(N)}$ replaces \mathcal{P} identically, but it completely rejects fine phase-space structures that cannot be expanded in terms of these N functions.

The truncation of \mathcal{P} to finite size breaks unitarity. Therefore, $\mathcal{P}^{(N)}$ may not only have unimodular eigenvalues but also eigenvalues located inside the unit circle. Furthermore, the spectrum of $\mathcal{P}^{(N)}$ is purely discrete. The N -dependence of the eigenvalues of $\mathcal{P}^{(N)}$ yields information on the spectral properties of \mathcal{P} . Upon diagonalizing $\mathcal{P}^{(N)}$ and increasing N we find the “newly born” eigenvalues close to the origin while the “older” ones move about in the complex plane. “Very old” ones eventually settle for good. If the classical dynamics is integrable ($\tau = 0$ or $\beta_y = 0$),

the asymptotic large- N loci are back to the unit circle, where the full \mathcal{P} has its discrete eigenvalues. The situation is different for the mixed phase space: while some eigenvalues of $\mathcal{P}^{(N)}$ “freeze” with unit moduli, others come to rest inside the unit circle as $N \rightarrow \infty$. These eigenvalues reflect resonances of \mathcal{P} in a higher Riemannian sheet of the complex plane. We see this phenomenon as analogous to the spectral concentration in perturbation theory [14,7,15]: a perturbation series for an operator with continuous spectrum does not converge but produces, with increasing order, a sequence of points concentrated in the neighborhood of the respective resonance.

An additional intuitive argument for the persistence of non-unimodular eigenvalues as $N \rightarrow \infty$ for nonintegrable dynamics is the following: in contrast to regular motion, chaos comes with a hierarchy of phase-space structures which extends without end to ever finer scales. Probability that is propagated from large to fine scales mostly does not return. This effectively dissipative character of the conservative dynamics is accounted for as true dissipation by the truncated propagator and its nonunimodular eigenvalues, but the difference between effective and true dissipation is irrelevant for low resolution. Moreover, a frozen nonunimodular eigenvalue is to be understood as a scale-independent dissipation rate, in tune with the expected selfsimilarity in phase space.

The freezing of non-unimodular eigenvalues is illustrated for two kicked tops, one with weakly chaotic ($\tau = 2.1$) and one with strongly chaotic character ($\tau = 10.2$). Figures 1a and 1b show the respective phase-space portraits. While for $\tau = 2.1$ large islands of regular motion still exist, for $\tau = 10.2$ regular islands have become so small that they are difficult to detect and impossible to resolve with $l_{\max} = 70$. Figures 2a and 2b show grey-shade coded histograms in the complex plane for the number of eigenvalues with moduli larger than 0.2 of all matrices with $l_{\max} = 40, 41, 42, \dots, 70$. Eigenvalues with moduli smaller than 0.2 are rejected because they have not settled yet and their density near the origin is so high that they would spoil the histogram. Large amplitudes (black) in the histograms indicate the positions of frozen eigenvalues. While for $\tau = 2.1$ a large number of frozen eigenvalues is found close to the unit circle, in the case $\tau = 10.2$, where no regular islands can be resolved, the only unimodular eigenvalue is the one at unity which pertains to the stationary uniform eigenfunction Y_{00} ; all other frozen eigenvalues lie well inside the unit circle and indicate resonance positions. Table I lists some of these frozen nonunimodular eigenvalues at resolutions $l_{\max} = 30, 40, 50$ and 60.

At first sight the two cases presented above may appear to correspond to quite different types of dynamics, but actually this is only a matter of resolution. As resolution is further increased in the strongly chaotic case ($\tau = 10.2$), elliptic islands will be resolved at some stage. Correspondingly, eigenvalues of $\mathcal{P}^{(N)}$ will emerge which freeze on the unit circle. Also new nonunimodular frozen eigenvalues may appear, possibly even ones larger in modulus than the frozen eigenvalues found at lower resolution.

IV. EIGENFUNCTIONS AND RESONANCE-EIGENFUNCTIONS AT FINITE PHASE-SPACE RESOLUTION

An investigation of the eigenfunctions of $\mathcal{P}^{(N)}$ reveals more about the nature of the frozen eigenvalues. Eigenvalues freezing with unit moduli have eigenfunctions located on elliptic islands of regular motion surrounding elliptic periodic orbits in phase space. Such islands are bounded by invariant tori which form impenetrable barriers in phase space. Thus if $\chi_{p,n}$ is a characteristic function constant on an island around the n th point of an p -periodic orbit and zero outside with $\chi_{p,n+1} = \mathcal{P}\chi_{p,n}$ and $\chi_{p,1} = \mathcal{P}\chi_{p,p}$, then

$$f_p = \sum_{n=1}^p \chi_{p,n} \quad (11)$$

is an eigenfunction of \mathcal{P} with eigenvalue unity. Moreover, linear combinations of such functions are eigenfunctions as well. Figures 3a,b show two eigenfunctions of $\mathcal{P}^{(N)}$ with eigenvalues 0.999976 and 0.999974 almost at unity for the kicked top with $\tau = 2.1$ and $l_{\max} = 60$. Amplitudes of the functions are large in dark shaded areas of phase space. The elliptic islands supporting the eigenfunctions can easily be identified in the phase-space portrait in figure 1a.

For $p > 1$ we furthermore expect and find the p th roots of unity as eigenvalues as well with eigenfunctions that have constant moduli on elliptic islands and are invariant under \mathcal{P}^p ,

$$f_{p,m} = \sum_{n=1}^p e^{i2\pi mn/p} \chi_{p,n}, \quad \text{with } m = 1, \dots, p. \quad (12)$$

Superpositions of two such $f_{p,m}, f_{p',m'}$ are also eigenfunctions if $m/p = m'/p'$, i.e. if all periods p' involved are multiples of p ; the possible phases are dictated by the shortest period p .

Once freezing has been observed for eigenvalues with moduli smaller than unity their eigenfunctions have approached their final shape on the resolved phase-space scales. In contrast to the eigenfunctions with unimodular eigenvalues these eigenfunctions are localized around unstable manifolds of hyperbolic periodic orbits, ones with low periods at first since these are easiest to resolve. [Typically, for every period several neighbouring orbits of approximately equal instability can be identified in an eigenfunction, their number being the larger the more extended the eigenfunction.] Figure 4 shows moduli of eigenfunctions for some of the nonunimodular eigenvalues listed in table I at resolution $l_{\max} = 60$. Particularly in figures 4b,c the localization on orbits of length six and four respectively is obvious. With growing l_{\max} more orbits of higher periods appear in the eigenfunction. Their supports gain complexity, in correspondence with the infinitely convoluted shape of the unstable manifolds. Just as for the eigenvalues there is no strict convergence of the eigenfunctions. Since no finite approximation $\mathcal{P}^{(N)}$ accounts for arbitrarily fine structures one encounters the aforementioned loss of probability from resolved to unresolved scales. Not even in the limit $N \rightarrow \infty$ can the unitarity of \mathcal{P} be restored: rather, in tune with a continuous spectrum of \mathcal{P} , the eigenfunctions tend to singular objects outside the Hilbert space. This becomes even more obvious in a comparison of eigenfunctions of $\mathcal{P}^{(N)}$ with eigenfunctions of the truncated inverse propagator $\mathcal{P}^{-1(N)}$. Both matrices have the same frozen eigenvalues, but only for the unimodular ones eigenfunctions of $\mathcal{P}^{(N)}$ and $\mathcal{P}^{-1(N)}$ to the same eigenvalue have (roughly) the same support, as it is expected for unitary dynamics: the elliptic islands that support the eigenfunctions are invariant under time reversal. For nonunimodular frozen eigenvalues eigenfunctions of $\mathcal{P}^{(N)}$ and $\mathcal{P}^{-1(N)}$ have distinct supports. While unstable periodic orbits are traversed in the opposite direction but remain the same under time reversal, stable and unstable manifolds are interchanged. Thus the eigenfunctions of $\mathcal{P}^{-1(N)}$ are localized near the same periodic orbits but around the stable manifolds of the forward-dynamics. In particular the eigenfunctions do not converge to the same limit as $N \rightarrow \infty$. Needless to say this again reflects the effective irreversibility of the chaotic Hamiltonian dynamics. Figures 5 and 6 illustrate the aforesaid. The eigenfunction in figure 5a at resolution $l_{\max} = 30$ corresponds to the same frozen eigenvalue as the eigenfunction in figure 5b at resolution $l_{\max} = 60$. While coarse structures are the same in both eigenfunctions, more fine structures appear at the higher resolution. Figure 5c shows, again for the same eigenvalue, the eigenfunction of $\mathcal{P}^{-1(N)}$ at $l_{\max} = 60$. In contrast to figure 5b localization is now on the stable manifolds of the same periodic orbits of the forward dynamics. These periodic orbits as well as their unstable and stable manifolds are shown in figure 6.

Just like the unimodular eigenvalues, frozen eigenvalues inside the unit circle come in p -families, i.e. with phases corresponding to the p th roots of unity, determined by the length p of the shortest periodic orbit present in an eigenfunction. Now the above argument must be modified in the following way: assume an eigenfunction f is mostly concentrated around a shortest unstable orbit with period p as well as a longer one with period p' . Denote by $\psi_{p,n}$ again a “characteristic function”, now constant near the n -th point of the period- p orbit, $n = 1 \dots p$, and zero elsewhere. The truncated Frobenius-Perron operator $\mathcal{P}^{(N)}$ maps $\psi_{p,n}$ into $\mathcal{P}^{(N)}\psi_{p,n} = r_p\psi_{p,n+1}$ with the real positive factor r_p smaller than unity accounting for losses, in particular to unresolved scales. As previously, independent linear combinations of the $\psi_{p,n}$ can be formed as

$$f_{p,m} = \sum_{n=1}^p e^{i2\pi mn/p} \psi_{p,n} \quad \text{with } m = 1 \dots p. \quad (13)$$

Now consider a sum of two such functions, $g = f_{p,m} + f_{p',m'}$, and apply $\mathcal{P}^{(N)}$. For g to qualify as an approximate eigenfunction we must obviously have $r_p \approx r_{p'}$, i.e. the two periodic orbits must be similarly unstable, and $m/p = m'/p'$. But then indeed $\mathcal{P}^{(N)}g \approx r_p e^{i2\pi m/p} g$ and $[\mathcal{P}^{(N)}]^p g \approx r_p^p g$, and the phase is dictated by the shortest orbit. Since orbits of low period are most likely to be resolved first, usually the first frozen eigenvalues found from diagonalizing $\mathcal{P}^{(N)}$ have phases corresponding to small numbers p . Since nonunimodular eigenvalues with phases according to $p = 1, 2, 4$ have already been presented in [12], in this paper we intentionally chose $\tau = 10.2$, a case for which eigenvalues with other phases happen to be more easily detected. In figure 2b and table I complex eigenvalues with phases near the sixth roots of unity are clearly visible.

V. PERIODIC-ORBIT EXPANSION OF THE SPECTRAL DETERMINANT

Since the unstable periodic orbits that are linked to a nonunimodular eigenvalue can be identified quite easily from the eigenfunction of $\mathcal{P}^{(N)}$, one is tempted to adopt a cycle expansion to calculate decay rates from periodic orbits.

For purely hyperbolic systems, cycle expansions of the spectral determinant, i.e. the characteristic polynomial of the Frobenius-Perron operator

$$d(z) = \det(1 - z\mathcal{P}) = \exp \operatorname{tr} \ln(1 - z\mathcal{P}) \quad (14)$$

are known to allow for the calculation of resonances with high accuracy [16,17]. The spectral determinant is expressed in terms of the traces of the Frobenius-Perron operator $\operatorname{tr} \mathcal{P}^n$ as

$$d(z) = \prod_{n=1}^{\infty} \exp \left(-\frac{z^n}{n} \operatorname{tr} \mathcal{P}^n \right) \quad (15)$$

and subsequently expanded as a finite polynomial up to some order n_{\max} . Only the first n_{\max} traces are required for the calculation of this polynomial, and only periodic orbits with primitive periods up to n_{\max} contribute to it.

The traces

$$\operatorname{tr} \mathcal{P}^n = \int dX \delta(X - M^n(X)) \quad (16)$$

are calculated as sums over hyperbolic periodic orbits of length n as

$$\operatorname{tr} \mathcal{P}^n = \sum_{X=M^n X} \frac{1}{|\det(1 - \Xi_n)|} \quad (17)$$

where the matrix $\Xi_n = \partial M^n(X)/\partial X$ is the linearized version of the map M^n evaluated at any of the points of a period- n orbit. If n is the r -fold of a primitive period p , the matrix Ξ_n can as well be written as $\Xi_n = \Xi_p^r$, and the spectral determinant as a product of contributions from all primitive orbits $\{k\}$,

$$d(z) = \prod_{\{k\}} \exp \left[-\sum_{r=1}^{\infty} \frac{1}{r} \frac{z^{pkr}}{\det(1 - \Xi_{pk}^r)} \right]. \quad (18)$$

The zeros z_i of the polynomial which are insensitive against an increase of n_{\max} are inverses of resonances.

For the ordinary cycle expansion of a spectral determinant just sketched to converge, all periodic orbits must be hyperbolic and sufficiently unstable [1,16,17]. These conditions are not met for a mixed phase space, not only because of the presence of elliptic orbits but also because of very weakly unstable orbits with high periods. We can circumvent such limitations by considering only one ergodic region in phase space at a time, bar contributions from elliptic orbits, and impose a stability bound by including only the relatively few, about equally unstable hyperbolic orbits $\{k\}_i$ identified in an eigenfunction of $\mathcal{P}^{(N)}$. We surmise that the spectral determinant factors as

$$d(z) = \prod_{i=1}^{\infty} d_i(z), \quad (19)$$

with one factor d_i for the family $\{k\}_i$ of periodic orbits showing up in the i th eigenfunction. Each such factor $d_i(z)$ is then calculated separately with the above expressions. Obviously this variant of the cycle expansion reproduces the phases of the resonances exactly since these are again directly determined by lengths of orbits: if p is the smallest period used in $d_i(z)$, the polynomial can as well be written as a polynomial in z^p thus allowing the zeros to have the phases of the p th roots of unity. Needless to say, the notorious proliferation of periodic orbits with growing length causes more and more difficulties for the cycle expansion for p -families of resonances with increasing p .

We first turn to the top with $\tau = 10$. Here, unstable orbits with periods 1, 2, and 4 and the corresponding p -families of resonances are easily detected. In Table II frozen eigenvalues found at the resolution $l_{\max} = 60$ are listed in the first column. The columns to the right show the corresponding results of the cycle expansion up to order $n_{\max} = 1, 2, 4$. The total number of orbits used in each case is given in curly brackets. For instance, our cycle expansion of the resonance 0.81 involves three orbits of lengths 1, 2 and 4. The resonance -0.7510 as well as its phase-related partners $-0.0079 \pm i0.7517$ can be approximately reproduced using four orbits of length 4. For the real positive eigenvalue 0.7470 (not listed in table II) completing this quartet of eigenvalues the eigenfunction is also localized in other regions of phase space and thus further orbits with periods different from $p = 4$ would have to be included in the cycle expansion. The first repetition of the single period-2 orbit contributing to the resonance 0.6597 in table II gives an almost diverging contribution to the spectral determinant, thus hindering its expansion to a higher order.

The top with $\tau = 10.2$ offers itself for a study of complex frozen eigenvalues with phases near the fourth and sixth roots of unity. Even though these two groups of eigenvalues are almost equal in modulus, the corresponding eigenfunctions are localized in different regions of phase space, and therefore the two examples turn out independent

(see figures 4b,c). The reason why we leave aside the eigenvalues on the real axis is that their eigenfunctions show localization on many orbits of different, higher periods which cannot all be identified (see figures 4a,d). For the resonances $-0.0058 \pm i0.7080$ the spectral determinant of order $n_{\max} = 4$, calculated from six periodic orbits of length 4, yields $\pm i0.8150$. In the next higher order $n_{\max} = 8$ another 9 orbits of primitive length 8 must be taken into account with the resulting approximants $\pm i0.7678$. For the resonances $0.3550 \pm i0.6199$ and $-0.3388 \pm i0.6243$ with phases near the sixth roots of unity 12 orbits of primitive length 6 contribute to the spectral determinant in lowest order. These orbits are shown in figure 6a. In lowest order the resulting six approximants of modulus 0.8599 still differ by about 20% from the respective moduli 0.7144 and 0.7103. These results are compiled in Table III.

VI. RESONANCES VERSUS CORRELATION DECAY

To check on the physical meaning of frozen eigenvalues with moduli smaller than unity as Frobenius-Perron resonances we propose to compare their moduli with rates of correlation decay. In a numerical experiment we investigate the decay of the correlator

$$C(n) = \frac{\langle \rho(n)\rho(0) \rangle - \langle \rho(\infty)\rho(0) \rangle}{\langle \rho(0)^2 \rangle - \langle \rho(\infty)\rho(0) \rangle}. \quad (20)$$

The initial densities $\rho(0)$ are chosen as characteristic functions on a grid of 2000×2000 cells in phase space. Each cell is represented by its central point $(q, p)_c$, and its temporal successor after one time step is the cell containing $M((q, p)_c)$. After n iterations we obtain $\rho(n)$. From the phase-space average $\langle \rho(n)\rho(0) \rangle$ we subtract the correlations remaining at $n = \infty$ due to the compactness of the phase space, and subsequently normalize.

Depending on the choice of $\rho(0)$ different long-time decays are observable. We choose $\rho(0)$ as covering the regions where the hyperbolic orbits relevant for a given resonance are situated. The long-time decay turns out insensitive to the exact choice of $\rho(0)$, provided $\rho(0)$ does not extend to phase-space regions supporting different eigenfunctions with frozen eigenvalues of larger moduli. Since $\rho(0)$ is real and positive, and positivity is preserved under the time evolution, we find positive real decay factors $C(n+1)/C(n)$. Indeed, after two or three time steps these decay factors are in rather good agreement with the modulus of the corresponding nonunimodular eigenvalue as well as with the result of our cycle expansion. Tables II and III list the decay factors we obtained from a numerical fit of $C(n)$ from $n = 2$ to $n = 18$, together with the moduli of the respective resonances. Figure 7 shows the decay of $C(n)$ (dots), with $\rho(0)$ chosen according to the eigenfunction shown in figure 4b. The numerical fit (line) yields a decay factor 0.7706, to be compared with 0.7103 as the modulus of the eigenvalue.

VII. CONCLUSIONS

In conclusion, we have presented a method to determine Frobenius-Perron resonances and eigenvalues which is applicable to systems with a mixed phase space. Resonances as well as eigenvalues are identified as frozen eigenvalues of a truncated propagator matrix $\mathcal{P}^{(N)}$ in a Hilbert space of phase-space functions. The corresponding eigenfunctions of $\mathcal{P}^{(N)}$ are strongly localized on the associated phase-space structures, elliptic islands for eigenvalues and unstable manifolds of hyperbolic periodic orbits for resonances. The expected characteristics of the resonance eigenfunctions, an infinite hierarchy of structures and the distinct supports of forward and backward time evolution, are clearly visible. The resonances obtained can be reproduced by a variant of the cycle expansion in which only the orbits that are identified in the eigenfunctions are taken into account. Finally, the correlation decay within a phase-space region that an eigenfunction is localized in is well predicted by the corresponding resonance. The cycle expansion as well as the observation of correlation decay may be used to check the accuracy of the resonances obtained as frozen eigenvalues. An accurate knowledge of the relevant resonances of mixed dynamics at a certain phase-space resolution is a desirable piece of information for many further investigations such as the role of classical resonances in quantum dynamics.

We are grateful to Shmuel Fishman for discussions initiating as well as accompanying this work. Support by the Sonderforschungsbereich ‘‘Unordnung und groÙe Fluktuationen’’ and the Minerva foundation is thankfully acknowledged.

VIII. APPENDIX A: MATRIX ELEMENTS OF THE FROBENIUS-PERRON OPERATOR

We here derive the matrix elements (6) of the Frobenius-Perron operator \mathcal{P} . It is convenient to use the representation of Y_{lm} in terms of associated Legendre Polynomials $P_l^m(x)$ [19],

$$Y_{lm}(q, p) = (-1)^m \left[\frac{2l+1}{4\pi} \frac{(l-m)!}{(l+m)!} \right]^{\frac{1}{2}} P_l^m(p) e^{imq}, \quad (21)$$

For rotations R_y, R_z and torsion T_z on the unit sphere the explicit forms for M read

$$\begin{aligned} R_y(\beta_y) : \begin{pmatrix} q \\ p \end{pmatrix} &\mapsto \begin{pmatrix} \arg \left(\sqrt{1-p^2} (\cos \beta_y \cos q + i \sin q) + p \sin \beta_y \right) \\ p \cos \beta_y - \sqrt{1-p^2} \sin \beta_y \cos q \end{pmatrix} \\ R_z(\beta_z) : \begin{pmatrix} q \\ p \end{pmatrix} &\mapsto \begin{pmatrix} q + \beta_z \\ p \end{pmatrix} \\ T_z(\tau) : \begin{pmatrix} q \\ p \end{pmatrix} &\mapsto \begin{pmatrix} q + \tau p \\ p \end{pmatrix}. \end{aligned} \quad (22)$$

The above immediately implies the intuitive result for the z -rotation

$$Y_{lm}(R_z^{-1}(q, p)) = e^{-im\beta_z} Y_{lm}(q, p). \quad (23)$$

Due to the orthonormality of the spherical harmonics we then find the Frobenius-Perron operator represented by the diagonal matrix

$$\exp(\mathcal{L}_{R_z})_{l_1 m_1, l_2 m_2} = \delta_{l_1 l_2} \delta_{m_1 m_2} e^{-im_2 \beta_z}. \quad (24)$$

Obviously and intuitively, $\exp(\mathcal{L}_{R_z})$ is identical to the quantum mechanical ($\hbar = 1$) rotation matrix $\langle l_1 m_1 | \exp(-i\beta_z L_z) | l_2 m_2 \rangle$ involving the L_z -component of the angular momentum operator $\vec{L} = (L_x, L_y, L_z)^T$ and the eigenbasis $Y_{lm} = |lm\rangle$ with $\vec{L}^2 |lm\rangle = l(l+1) |lm\rangle$ and $L_z |lm\rangle = m |lm\rangle$. Since this formal identity holds for the z -rotation it must also hold for the y -rotation. Thus for $\exp(\mathcal{L}_{R_y})$ we must take the representation of the quantum operator $\exp(-i\beta_y L_y)$, well known as Wigner's d -matrix,

$$\exp(\mathcal{L}_{R_y})_{l_1 m_1, l_2 m_2} = \langle l_1 m_1 | \exp(-i\beta_y L_y) | l_2 m_2 \rangle = \delta_{l_1 l_2} d_{m_1 m_2}^{l_1}(\beta_y), \quad (25)$$

which can be obtained from recursion relations [18]. This matrix is still diagonal in l_1, l_2 . In fact, the Frobenius-Perron matrix for any rotation is diagonal in that pair of indices. An immediate implication is that pure rotations do not couple the subspace of Y_{lm} with $l \leq l_{\max}$ to its complement. For the integrable dynamics of rotation no probability is dissipated from the subspace and the spectrum of $\mathcal{P}^{(N)}$ lies exactly on the unit circle.

For the z -torsion we make the replacement

$$Y_{lm}(T_z^{-1}(q, p)) = e^{-i\tau m p} Y_{lm}(q, p) \quad (26)$$

in the phase-space integral (6) and then use the expansion [20]

$$e^{-ik \cos \theta} = \sum_{l=0}^{\infty} (-i)^l \sqrt{4\pi(2l+1)} j_l(k) Y_{l0}(\varphi, \cos \theta), \quad (27)$$

which involves the spherical Bessel function $j_l(k)$. The parity $Y_{l_1 m_1}^* = (-1)^{m_1} Y_{l_1, -m_1}$ helps us on to

$$\exp(\mathcal{L}_{T_z})_{l_1 m_1, l_2 m_2} = (-1)^{m_1} \sum_{l=0}^{\infty} (-i)^l \sqrt{4\pi(2l+1)} j_l(m_1 \tau) \int_{\Omega} dq dp Y_{l0} Y_{l_1, -m_1} Y_{l_2 m_2}. \quad (28)$$

We here meet Gaunt's integral [21] over three spherical harmonics which can be written in terms of two Clebsch-Gordan coefficients,

$$\int_{\Omega} dq dp Y_{lm}^* Y_{l_1 m_1} Y_{l_2 m_2} = \left[\frac{(2l_1+1)(2l_2+1)}{4\pi(2l+1)} \right]^{\frac{1}{2}} C_{000}^{l_1 l_2 l} C_{m_1 m_2 m}^{l_1 l_2 l}. \quad (29)$$

Finally, using the following properties of Clebsch-Gordan coefficients,

$$\begin{aligned} C_{m_1 m_2 m}^{l_1 l_2 l} &= 0 \quad \text{if } l \notin \{(l_1 + l_2), (l_1 + l_2) - 1, \dots, |l_1 - l_2|\}, \\ C_{m_1 m_2 m}^{l_1 l_2 l} &= 0 \quad \text{if } m_1 + m_2 \neq m, \\ C_{0 0 0}^{l_1 l_2 l} &= 0 \quad \text{if } l_1 + l_2 + l \text{ odd} \end{aligned} \quad (30)$$

the infinite sum in (28) can be reduced to a finite one,

$$\exp(\mathcal{L}_{T_z})_{l_1 m_1, l_2 m_2} = \delta_{m_1 m_2} (-1)^{m_1} \sqrt{(2l_1 + 1)(2l_2 + 1)} \sum_{l=|l_1 - l_2|}^{l_1 + l_2} (-i)^l j_l(m_1 \tau) C_{0 0 0}^{l_1 l_2 l} C_{-m_1 m_2 0}^{l_1 l_2 l}. \quad (31)$$

It is worth noting that due to the properties (30) the matrix elements (31) are real if $l_1 + l_2$ is even or purely imaginary if $l_1 + l_2$ is odd. Furthermore they are symmetric with respect to l_1 and l_2 .

IX. APPENDIX B: RECURSION RELATION FOR THE TORSION MATRIX ELEMENTS

A recursion relation similar to the recursion relation used to calculate Wigner's d-matrix can be derived for the torsion matrix elements. For simplicity we consider the integral

$$t_z(l', l, m) = \int_{-1}^1 du P_{l'}^m(u) e^{i\tau m u} P_l^m(u) \quad (32)$$

which is related to the torsion matrix elements by

$$\exp(\mathcal{L}_{T_z})_{l' m l m} = \frac{1}{2} \left[\frac{(2l' + 1)(l' - m)! (2l + 1)(l - m)!}{(l' + m)! (l + m)!} \right]^{\frac{1}{2}} t_z(l', l, m). \quad (33)$$

The associated Legendre polynomials obey the differential equation

$$D P_l^m(u) \equiv \left[(1 - u^2) \frac{d^2}{du^2} - 2u \frac{d}{du} + l(l + 1) - \frac{m^2}{1 - u^2} \right] P_l^m(u) = 0. \quad (34)$$

This suggests to draw a recursion relation from

$$\int_{-1}^1 du [D P_{l'}^m(u)] P_l^m(u) e^{i\tau m u} = 0. \quad (35)$$

In the case $m \neq 0$ integration by parts leads to

$$\begin{aligned} \int_{-1}^1 du P_{l'}^m e^{i\tau m u} \left[(2i\tau m) \left((1 - u^2) \frac{d}{du} P_l^m - u P_l^m \right) + \right. \\ \left. (l'(l' + 1) - l(l + 1) - (1 - u^2) \tau^2 m^2) P_l^m \right] = 0. \end{aligned} \quad (36)$$

Now with the help of the identity

$$(1 - u^2) \frac{d}{du} P_l^m = -l u P_l^m + (l + m) P_{l-1}^m \quad (37)$$

the derivative in (36) can be eliminated and we arrive at the five-step recursion relation

$$\begin{aligned} t_z(l', l + 2, m) &= \frac{1}{\tau^2 m^2} \frac{(2l + 1)(2l + 3)}{(l - m + 1)(l - m + 2)} \left[2i\tau m \frac{(l + 1)(l - m + 1)}{2l + 1} t_z(l', l + 1, m) \right. \\ &\quad - \left(l'(l' + 1) - l(l + 1) - 2\tau^2 m^2 \frac{l(l + 1) + m^2 - 1}{4l(l + 1) - 3} \right) t_z(l', l, m) \\ &\quad \left. - 2i\tau m \frac{l(l + m)}{2l + 1} t_z(l', l - 1, m) - \tau^2 m^2 \frac{(l + m)(l + m - 1)}{(2l + 1)(2l - 1)} t_z(l', l - 2, m) \right]. \end{aligned} \quad (38)$$

For constant indices l' and $m \neq 0$ this links matrix elements with five successive values of the index l . Just like the torsion matrix elements for these indices the terms in the recursion relation have alternately real and imaginary values. Even though the recursion relation involves five matrix elements, only two integrals have to be done initially. These are the nonvanishing integrals $t_z(l', |m|, m)$ and $t_z(l', |m| + 1, m)$ for the smallest values of l . Together with $t_z(l', |m| - 1, m) = 0$ and $t_z(l', |m| - 2, m) = 0$ they can be used to start the recursion.

For $m = 0$ the recursion formula does not apply, but the integral

$$t_z(l', l, 0) = \frac{2}{2l+1} \delta_{l'l'} \quad (39)$$

is trivial in this case.

- [1] D. Ruelle, Phys. Rev. Lett. **56**, 405 (1986); D. Ruelle, J. Stat. Phys. **44**, 281 (1986).
- [2] M. Pollicott, Invent. Math. **81**, 415 (1985)
- [3] F. Haake, C. Manderfeld, J. Weber, and P. A. Braun, in preparation
- [4] K. Pance, W. Lu, S. Sridhar, Phys. Rev. Lett. **85**, 2737 (2000)
- [5] A. V. Andreev and B. L. Altshuler, Phys. Rev. Lett. **75**, 902 (1995); O. Agam, B. L. Altshuler, and A. V. Andreev, Phys. Rev. Lett. **75**, 4389 (1995); A. V. Andreev, O. Agam, B. D. Simons, and B. L. Altshuler, Phys. Rev. Lett. **76**, 3947 (1996); A. V. Andreev, B. D. Simons, O. Agam, and B. L. Altshuler, Nuclear Physics B, **482**, 536 (1996).
- [6] M. R. Zirnbauer in: I.V. Lerner, J.P. Keating, and D.E. Khmelnitskii (eds.), *Supersymmetry and Trace Formulae: Chaos and Disorder* (Kluwer Academic, New York, 1999)
- [7] M. Reed and B. Simon, *Methods of Modern Mathematical Physics IV: Analysis of Operators* (Academic Press, New York, 1978).
- [8] S. Fishman in: I.V. Lerner, J.P. Keating, and D.E. Khmelnitskii (eds.), *Supersymmetry and Trace Formulae: Chaos and Disorder* (Kluwer Academic, New York, 1999)
- [9] M. Khodas and S. Fishman, Phys. Rev. Lett. **84**, 2837 (2000); M. Khodas and S. Fishman, Phys. Rev. E **62**, 4769 (2000).
- [10] H. H. Hasegawa und W. C. Saphir, Phys. Rev. A **46**, 7401 (1992)
- [11] V. Baladi, J.-P. Eckmann, and D. Ruelle, Nonlinearity **2**, 119 (1989)
- [12] J. Weber, F. Haake, and P. Šeba, Phys. Rev. Lett. **85**, 3620 (2000)
- [13] F. Haake, *Quantum Signatures of Chaos, 2nd ed.* (Springer, Berlin, 2001)
- [14] E. C. Titchmarsh, Proc. Roy. Soc. London Ser. A **210**, 30 (1951)
- [15] T. Kato, *Perturbation Theory for Linear Operators* (Springer, Berlin, 1995)
- [16] P. Cvitanović et al., *Classical and Quantum Chaos: A Cyclist Treatise*, (Nils Bohr Institute, Copenhagen, 1999) (www.nbi.dk/ChaosBook/)
- [17] F. Christiansen, G. Paladin, and H. H. Rugh, Phys. Rev. Lett. **65**, 2087 (1990)
- [18] P. A. Braun, P. Gerwinski, F. Haake, and H. Schomerus, Z. Phys. B **100**, 115 (1996)
- [19] L. C. Biedenharn and J. D. Louck, *Encyclopedia of Mathematics and Its Applications: Angular Momentum in Quantum Physics* (Addison-Wesley, Reading, 1981)
- [20] I. S. Gradshteyn and I. M. Ryzhik, *Table of Series, Integrals, and Products* (Academic Press, San Diego, 1994)
- [21] J. A. Gaunt, Trans. Roy. Soc. A **228**, 151 (1929)

$l_{\max} = 30$	$l_{\max} = 40$	$l_{\max} = 50$	$l_{\max} = 60$
0.7700	0.7688	0.7523	0.7696
0.3075	0.3429	0.3523	0.3550
$\pm i 0.5740$	$\pm i 0.6140$	$\pm i 0.6211$	$\pm i 0.6199$
-0.3170	-0.3348	-0.3444	-0.3388
$\pm i 0.6003$	$\pm i 0.6272$	$\pm i 0.6283$	$\pm i 0.6243$
-0.0042	-0.0002	-0.0100	-0.0058
$\pm i 0.7161$	$\pm i 0.7133$	$\pm i 0.6930$	$\pm i 0.7080$
-0.7025	-0.7228	-0.7155	-0.7165
0.6544	0.6230	0.6495	0.6480
...	-0.5619	-0.5753	-0.5667

TABLE I. Frozen nonunimodular eigenvalues for $\tau = 10.2$ at $l_{\max} = 30, 40, 50$ and 60 that can be identified from the histogram shown in figure 2b.

$l_{\max} = 60$	$n_{\max} = 1$	$n_{\max} = 2$	$n_{\max} = 4$	Decay of $C(n)$
0.8103	0.2185{1}	0.7070{2}	0.7664{3}	0.8005
-0.7510	-0.7483{4}	0.7697
-0.0079	-0.7483{4}	0.7697
$\pm i 0.7517$	-0.7483{4}	0.7697
0.6597	...	0.4969{1}	...	0.6783

TABLE II. Left column: resonances obtained from the truncated propagator for $\tau = 10.0$ and $l_{\max} = 60$. Middle columns: corresponding results from cycle expansion up to order $n_{\max} = 1, 2, 4$. The total number of primitive orbits employed is given in curly brackets. The eigenvalues in the second and third row belong to the same quartet of phase-related partners. Right column: Associated decay factors by which $C(n)$ decreases over one time step, obtained from numerical fit.

$l_{\max} = 60$	$n_{\max} = 4$	$n_{\max} = 6$	$n_{\max} = 8$	Decay of $C(n)$
-0.0058	$\pm i 0.8150\{6\}$...	$\pm i 0.7678\{15\}$	0.7694
$\pm i 0.7080$...	0.4299	...	0.7706
0.3550	...	$\pm i 0.7447\{12\}$...	0.7706
$\pm i 0.6199$...	-0.4299	...	0.7706
-0.3388	...	$\pm i 0.7447\{12\}$...	0.7706
$\pm i 0.6243$...	$\pm i 0.7447\{12\}$...	0.7706

TABLE III. Left column: resonances obtained from the truncated propagator for $\tau = 10.2$ and $l_{\max} = 60$. Middle columns: corresponding results from cycle expansion up to order $n_{\max} = 4, 6, 8$. The total number of primitive orbits employed is given in curly brackets. The eigenvalues in the second and third row belong to the same sextet of phase-related partners. Right column: Associated decay factors by which $C(n)$ decreases over one time step, obtained from a numerical fit.

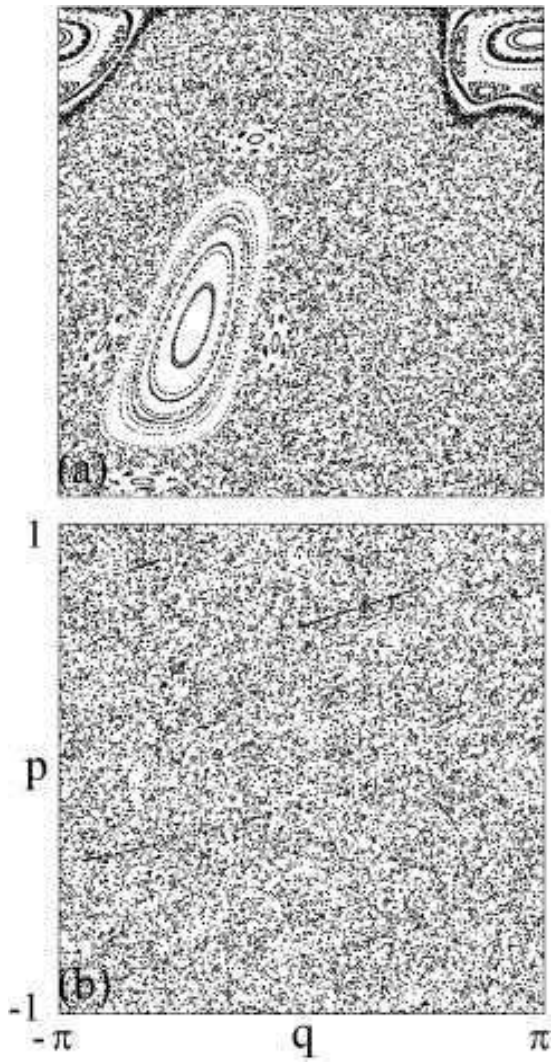


FIG. 1. Phase-space portraits of the weakly chaotic kicked top with torsion parameter $\tau = 2.1$ (a), and of the strongly chaotic top with $\tau = 10.2$ (b).

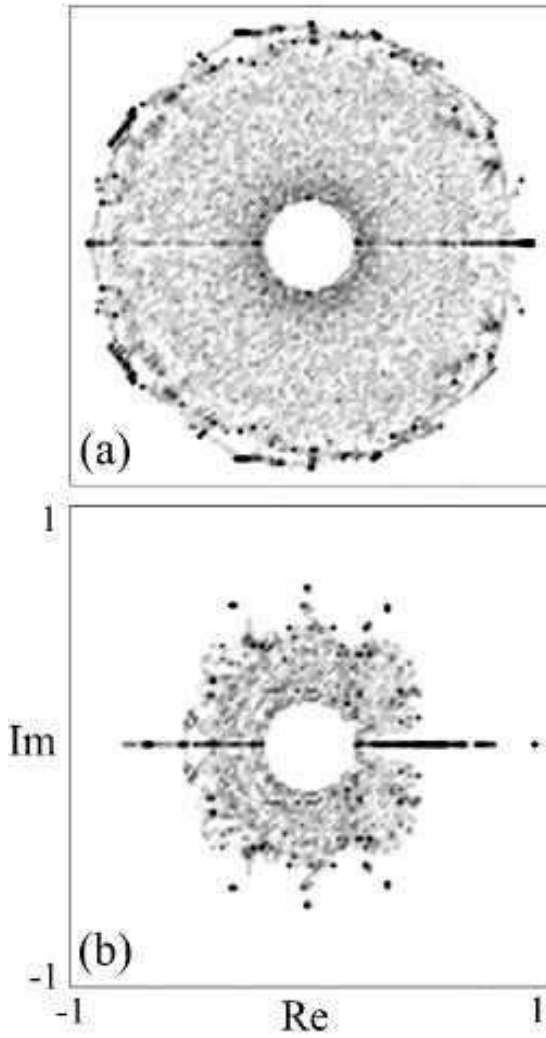


FIG. 2. Histograms showing the distributions of eigenvalues with moduli larger than 0.2 of all matrices with $l_{\max} = 40, 41, \dots, 70$ in the complex plane for $\tau = 2.1$ (a) and $\tau = 10.2$ (b). Large amplitudes (black) indicate positions of frozen eigenvalues.

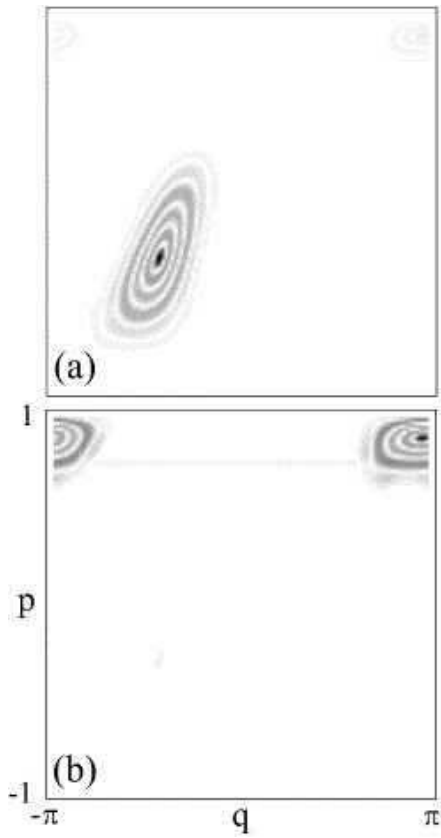


FIG. 3. Eigenvalues 0.999976 (a) and 0.999974 (b) almost at unity of $\mathcal{P}^{(N)}$ with $l_{\max} = 60$ in the weakly chaotic case $\tau = 2.1$ have eigenfunctions that are localized on elliptic islands. Dark-shaded regions in phase space indicate large amplitudes of the eigenfunctions.

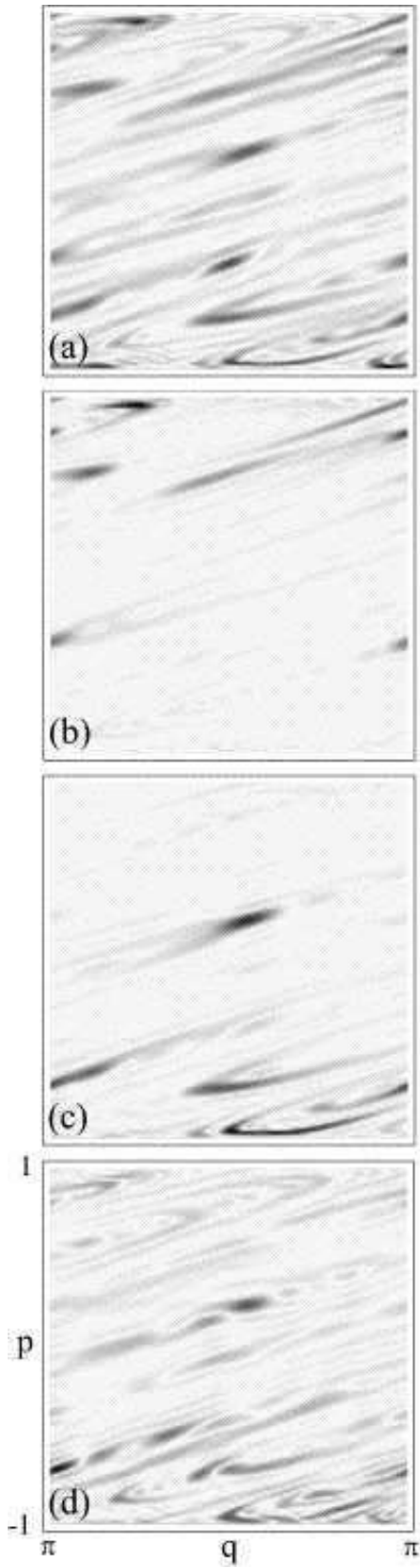


FIG. 4. For frozen eigenvalues 0.7696 (a), $-0.3388 \pm i0.6243$ (b), $-0.0058 \pm i0.7080$ (c), 0.6480 (d) of $\mathcal{P}^{(N)}$ ($\tau = 10.2$, $l_{\max} = 60$) inside the unit circle eigenfunctions have large amplitudes (dark-shaded areas) around unstable manifolds of hyperbolic periodic orbits in phase space.

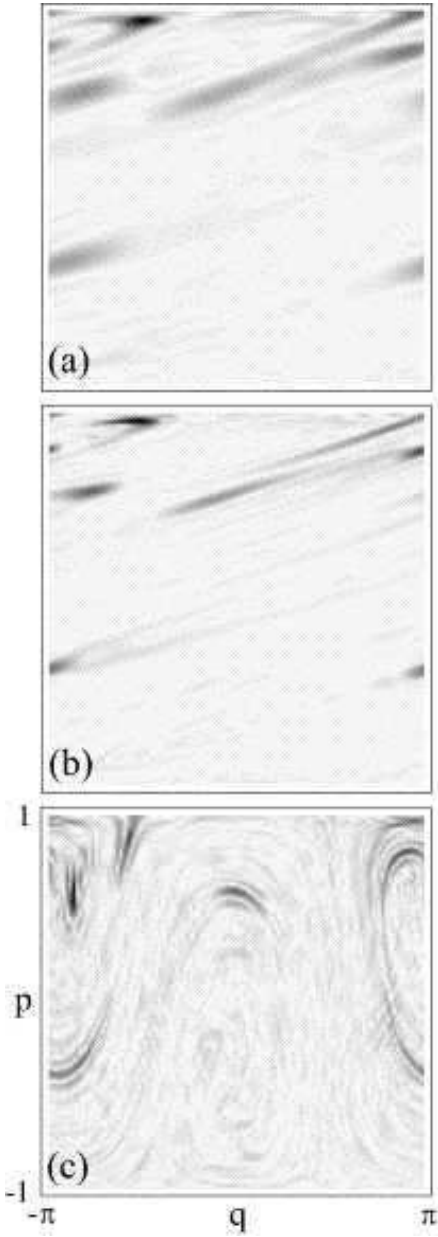


FIG. 5. As phase-space resolution increases from $l_{\max} = 30$ (a) to $l_{\max} = 60$ (b), the eigenfunction of $\mathcal{P}^{(N)}$ for the frozen nonunimodular eigenvalue $-0.3388 \pm i0.6243$ gains new structures on finer scales ($\tau = 10.2$). The corresponding eigenfunction (c) of $\mathcal{P}^{-1(N)}$ (resolution $l_{\max} = 60$) is localized at the same periodic orbit as the eigenfunction (b) but with stable and unstable manifolds interchanged. Therefore, see also figure 6a for the periodic orbits, figure 6b for the unstable and figure 6c for the stable manifolds; these manifolds are clearly dominating the present eigenfunction.

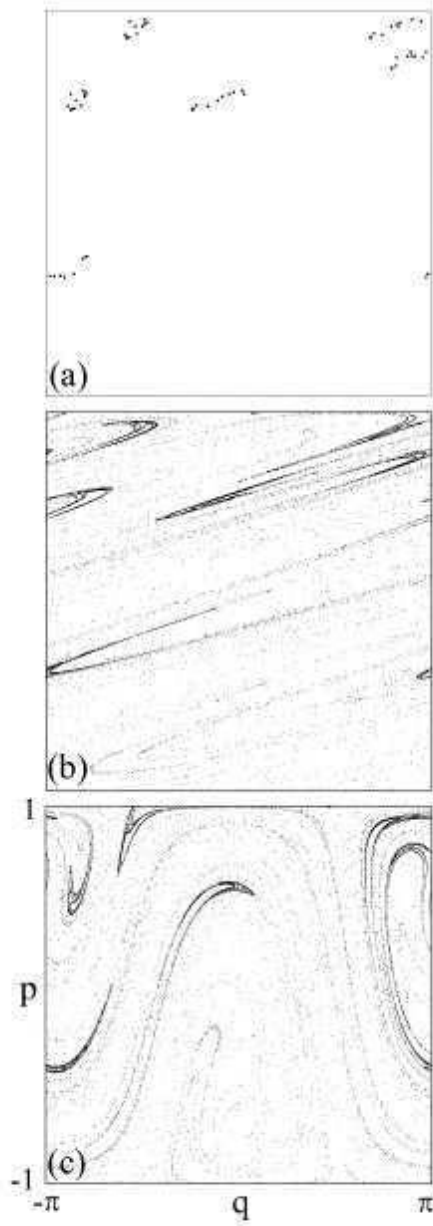


FIG. 6. (a): The 12 orbits of primitive length 6 that can be identified for the resonances $0.3550 \pm i0.6199$ and $-0.3388 \pm i0.6243$ with phases near the sixth roots of unity from the eigenfunction shown in figures 4b (also 5b). They contribute to the expansion of $d_i(z)$ in lowest order. The unstable manifolds of these orbits are shown in (b), the stable manifolds in (c).

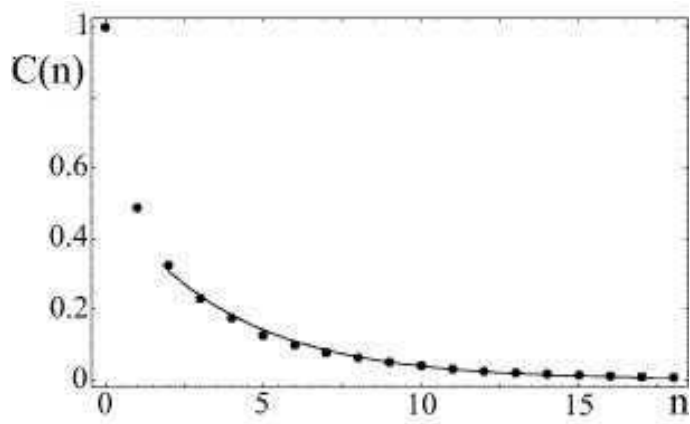


FIG. 7. Decay of $C(n)$ (dots) with $\rho(0)$ chosen according to the eigenfunction shown in figure 4b (also 5b). The numerical fit (line) yields a decay factor 0.7706.